LAWRENCE
LIVERMORE
NATIONAL
LABORATORY

LLNL-JRNL-612452

Solid-State Framing Camera with Multiple Time Frames

K. L. Baker, R. E. Stewart, P. T. Steele, S. P. Vernon, W. W. Hsing, B. A. Remington

January 23, 2013

Applied Physics Letters

Disclaimer

This document was prepared as an account of work sponsored by an agency of the United States government. Neither the United States government nor Lawrence Livermore National Security, LLC, nor any of their employees makes any warranty, expressed or implied, or assumes any legal liability or responsibility for the accuracy, completeness, or usefulness of any information, apparatus, product, or process disclosed, or represents that its use would not infringe privately owned rights. Reference herein to any specific commercial product, process, or service by trade name, trademark, manufacturer, or otherwise does not necessarily constitute or imply its endorsement, recommendation, or favoring by the United States government or Lawrence Livermore National Security, LLC. The views and opinions of authors expressed herein do not necessarily state or reflect those of the United States government or Lawrence Livermore National Security, LLC, and shall not be used for advertising or product endorsement purposes.

Solid-State Framing Camera with Multiple Time Frames

K.L. Baker, R.E. Stewart, P.T. Steele, S.P. Vernon, W.W. Hsing and B.A. Remington

Lawrence Livermore National Laboratory, Livermore, CA, USA

shot 254,255 May 16 2011.

Abstract

A high speed solid-state framing camera has been developed which can operate over a wide range of photon energies from the visible/near-infrared, 1.74 eV, into the hard x-ray regime, 10's of keV. This diagnostic uses the ultrafast index of refraction change in a single crystal cadmium selenide semiconductor. The index of refraction changes are due to the absorption of photons of higher energy than the bandgap of the semiconductor and this change is detected using a short pulse probe beam, ~500 fs, which is composed of photons with an energy lower than that of the bandgap. This camera measures the two-dimensional spatial profile of the flux incident of the cadmium selenide semiconductor at multiple times. This multi-frame camera has been tested at 3.1 eV using a frequency doubled Ti:Sapphire laser and at 4.5 keV and 8 keV using K_α emission from a titanium and copper laser-produced x-ray plasma source, respectively. The framing camera currently records two frames with a temporal separation between the frames of 5 ps but this separation can be varied between 100s of femtoseconds up to nanoseconds and the number of frames can be increased using an alternative approach to probing the cadmium selenide semiconductor. The use of a narrow bandgap semiconductor, rather than the current cadmium selenide would also enable the extension of this technique well

into the long-wavelength infrared spectrum, down to 12 um using $Hg_{0.8}Cd_{0.2}Te$ for instance.

Ultrafast pump-probe techniques have been developed in the visible and x-ray regime to study the dynamics of physical systems and achieve two-dimensional gated images. In the x-ray regime, using sub-ps free electron lasers (FEL), these pump-probe systems have generally measured the diffraction pattern of the FEL and reconstructed the object under study using iterative phase retrieval techniques which were originally developed by the electron and visible optics communities.[1-7] Also in the x-ray regime, laser-produced x-ray backlighters from short pulse lasers have been used to backlight imploding fusion capsules and Rayleigh-Taylor instability experiments to infer the two-dimensional line-averaged density in the target.[8-9] These laser-plasma experiments are limited to gate times defined by the temporal length of the x-ray source, several ps, and generally must be used with gated framing cameras in addition to block the x-ray emission from the target under study. These gated x-ray framing cameras have an inherent spatial resolution of ~50 um due to the microchannel plate technology employed.[10] These pump-probe techniques, however, require an active probe beam, either in the optical or x-ray regime, and can't be used for example to study the time dependent self-emission from the object under study. In addition many facilities, such as the National Ignition Facility, do not yet have access to short pulse lasers with sufficient energy to perform backlighting experiments.

In order to measure self-emission over a short period of time it is necessary to employ a gated detector. Current x-ray framing cameras use strip line microchannel

plates to achieve multiple frames of x-ray images. These devices are limited to temporal resolutions of ~30 to 40 picoseconds, ps, and as stated above the inherent spatial resolution of the detector itself is also limited to ~50 um due to the microchannel plate technology employed.[10] Intensified charge coupled devices, ICCDs, which also utilize microchannel plates, are used to take single frame optical images at temporal resolutions of ~1 nanosecond, ns, and a spatial resolution of >30 um. Pockels cells can be utilized in the optical and infrared to obtain gated images but they introduce a wavelength dependent transmission through the Pockels cell/polarizer combination and are limited to gates times longer than a nanosecond. There are currently no options for high speed, ps, framing cameras operating in the infrared spectrum.

The impetus behind the development of the framing camera described in this article was the need to have an x-ray framing camera that could measure the self-emission from imploding fusion capsules and the burn propagation of an ignited plasma. The requirements for such an x-ray imager include a high spatial resolution, ~5 um, a fast temporal resolution, several ps, and the ability to operate in a high neutron yield environment, approaching 10^{19} neutrons produced in a time of 15 to 20 psec. This neutron flux can interact directly with all elements of the diagnostics, overwriting electronically or photographically stored images before they can be read out.[11] When the neutrons reach the chamber wall or objects in the chamber, they promptly undergo (n,n`)γ reactions and produce a massive gamma ray flux throughout the vicinity of the target chamber. The gamma ray flux produces Cherenkov light in glass optics that can contaminate signals, and can darken optical fiber and glass at high exposure levels.[11] Calculations and tests of the interaction of neutrons with the chamber structure and

diagnostic elements predict that this gamma ray flux will produce sufficient EMP levels to generate large transient currents and voltages on exposed cables and electronics.[11] They are also likely to cause permanent failure of unshielded electronic devices and can affect the operation of electronic cameras that are exposed to it. Our approach to these challenging requirements was to develop a framing camera in which the two-dimensional x-ray flux would be rapidly encoded, < 1 ps, into an optical probe beam and then relay imaged out of the chamber and into a shielded bunker where it would be protected from the effects of these neutrons.

The framing camera described in this article represents a fundamental shift from the microchannel plate paradigm and accomplishes the functions of a framing camera with all optical and solid-state components. Some of the advantages of this approach include the ability to achieve higher spatial resolution than instruments utilizing a microchannel plate, temporal resolution approaching 100s of femtoseconds, potentially higher dynamic range and the ability to operate in a high neutron flux environment. In addition, with straightforward modifications the framing camera could be made to operate from the x-ray regime down to the long wavelength infrared spectrum and additional time frames, beyond the two current frames, could be implemented with inter-frame temporal spacing ranging from subpicosecond to nanoseconds. This broad functionality would find uses in many different areas of research.

The optical encoding of the x-ray flux is based upon the rapid change, <100 fs, in the index of refraction of a semiconductor when the semiconductor is excited with photons with energy higher than the bandgap. These incident photons create electrons and holes with excess energy which then relax through interactions with phonons and

other carriers in the system. The photoexcited carriers in the conduction and valence bands modify the absorption spectrum, which results in a change in the refractive index through the Kramers–Kronig relation between the real part of the refractive index and the absorption coefficient.[12] This change in the index of refraction is dependent on the probe energy, relative to the bandgap energy, and is highest for energies close to the bandgap in the semiconductor. The optical encoding itself is accomplished through the use of a binary grating, with a period of 20 μm, in contact with the semiconductor. When photons with an energy higher than the bandgap of the semiconductor pass through the binary grating and into the semiconductor they create a transient phase grating inside the semiconductor. A probe beam, composed of photons with an energy lower than the bandgap of the semiconductor, is then incident from the opposite side of the semiconductor as the pump source and probes the transient grating. This opposite side of the semiconductor has an antireflection, AR, coating for the probe wavelength. The side of the semiconductor in contact with the grating has a high reflectance, HR, coating for the probe wavelength such that the probe beam passes through the transient grating twice, the second time after reflecting off of the HR coating. The probe beam then leaves the semiconductor in the opposite direction from which it was incident. When the transient grating is present, the reflected probe beam consists of both the zero order component, specular, as well as the higher diffractive orders of the grating, each of which leaves the semiconductor at separate angles given by the grating equation.

Several techniques were employed to reduce scattered light and noise in the diffracted images. Noise can come from both the diffraction pattern of the probe beam and scattering caused by imperfections in the imaging optics and the semiconductor

internal structure and external surfaces. To address the diffraction pattern of the probe beam we employed an apodizer mask. Apodizers are used to change the distribution of diffracted light in the far-field.[13] The functional form of the apodizer pattern was chosen to be a discreet version of a Blackman window, whose continuous form satisfies the equation $T(r,\theta)=0.42-0.05\cos[2\pi(r+0.5)]+0.08\cos[4\pi(r+0.5)]$. For the apodizer used in this experiment, we implemented the continuous Blackman window as 360 separate leaves with each leaf representing one degree. The apodizer was made on a quartz substrate by over coating with chrome and then selectively removing the chrome using lithographic techniques. One of the 360 leaves comprising the apodizer is shown in Figure 1. this figure shows a closed curve representing 1 degree of the apodizer. All light on the outside of the closed curve was attenuated, $<10^{-5}$ transmission, by a thick chrome layer.

A second contribution to the scattered light seen in the images is due to scattered light, from the surface of the semiconductor itself and also due to imperfections in the crystal; grain boundaries, twinning planes, etc. Because of the cadmium in the semiconductor we were unable to polish the wafer at the time of the experiment. To reduce the level of scattered light from the as purchased wafer, a filter was placed in the Fourier plane to block the majority of the scattered light, as well as the zero order probe light, and only pass the signal from the odd orders of the transient grating diffraction pattern. In particular, the filter consisted of placing circular holes at the locations in the Fourier plane corresponding to the odd orders of the diffraction pattern as seen in figures 2 and 3. Because the bar and trough region of the gratings were of equal width, the even diffracted orders of the grating were expected to be weak relative to the odd orders and

were blocked. This eliminated the majority of the scattered light but also introduced a limit on the spatial resolution obtainable. The diameter of the hole was chosen to be the distance between the zero order and first order diffracted spots from the 20 um period x-ray grating. Therefore each of the holes passed spatial wavelengths larger than 40 um at the semiconductor plane(25 cycles/mm). The 2-D isotropic power spectral density function of polished optics generally follows a power law between, $k^{-1.5}$ to $k^{-2.5}$, where k represents a surface spatial frequency.[14,15] A Fourier plane camera was used to measure the scattered light in the Fourier plane at the location of the first and third orders of the x-ray diffraction grating and the scattered probe light within the Fourier plane filter around the third order was more than a magnitude lower than the scattered probe light within the Fourier plane filter encompassing the first order of the x-ray transient grating. As such by increasing the frequency of the x-ray modulation grating from a pitch of 20 um to a pitch of 4 um, a factor of 5, one would expect a decrease in the scattered light from the semiconductor surface between a factor of 11 to 56. That would likewise increase the spatial frequencies passed by the Fourier filter to 100 cycles/mm.

A wave-optics simulation was performed to demonstrate the effects of the apodizer on the ability of the system to measure small transient phase profiles. In particular a continuous Blackman apodizer was compared with a uniform circular aperture, both with and without a transient sinusoidal phase pattern, amplitude of 0.00628 radians, present in the cadmium selenide, CdSe. At this level the sinusoidal phase pattern is not observed above the diffraction pattern of the zero order beam in the case of the uniform circular aperture, Figure 2a, but is more than five orders of magnitude above the diffraction pattern from the zero order beam in the case of the Blackman apodized

aperture, Figure 2b. In these figures the only signal that is passed to the detector lies within the dashed black circle. The rest of the Fourier plane is blocked to suppress the zero order from the probe beam and the scattered light which originates from the external surfaces and from the internal imperfections of the semiconductor.

The experiments conducted to test this framing camera were carried out on the Callisto laser at the Lawrence Livermore National Laboratory's Jupiter Laser Facility. The experimental setup is shown in Figure 3. The short pulse probe beam, ~1 ps full-width-at-half-maximum, passed through the Blackman apodizer, through a half wave plate that was used to equilibrate the zero order probe energy between the two frames on the detector and then through a birefringent crystal which was used to introduce a time delay between the two orthogonally polarized probe signals. The probe was slightly chirped such that if the chirp were completely removed the pulse length would be ~60 fs. The delay crystal was an A-cut YVO_4 crystal which produced a relative delay between the two orthogonal polarizations of the probe beam of $(n_e-n_o)L/c$ or ~ 5 ps for the L=7 mm long crystal at the probe wavelength of 805 nm. The two temporally displaced probe beams then reflected off of the CdSe semiconductor. CdSe was chosen primarily due to the close proximity of its band gap energy, 1.74 eV, to the experimental facility's probe beam energy, 1.54 eV(805 nm). The CdSe semiconductor was AR coated for 805 nm on the side upon which the probe beam was incident. The side facing the source was coated with either a dielectric HR coating or 250 nm of copper to provide a reflective surface for the probe beam but to allow passage of the source photons(3.1 eV, 4.5 keV or 8 keV, respectively) into the CdSe semiconductor. A grating/mask was placed in contact with the HR layer to provide the spatial modulation of the impinging x rays or 400 nm photons

from the doubled Ti:Sapphire facility laser. The x-ray grating/mask was constructed by Microworks Gmbh with an overall pitch of 20 um, 10 um wide and 10 um thick gold bars with 10 um wide and 16 um thick epoxy resin in between the gold bars. A portion of the x-ray grating/mask is shown in Figure 4 showing resolution bars used to determine the modulation transfer function of the camera and a central National Ignition Facility, NIF, logo. The visible/ultraviolet grating consisted of a fused silica substrate with an aluminum binary grating which also had an overall pitch of 20 um, 10 um wide aluminum bars and 10 um wide AR coated fused silica. The probe beams were relay imaged from the CdSe convertor onto a beam displacer which was used to spatially separate the two orthogonally polarized probe beams. The two probe beams then passed through a Fresnel biprism to enable the two probe beams to be differentially filtered in the Fourier plane. These two temporally and spatially separated probe beams were then relay imaged onto the CCD detector which recorded the two images which were separated in time by ~ 5 ps. A beamsplitter was also used in conjunction with a lens to form two images, also separated in time by ~ 5 ps, of the Fourier plane on a separate CCD detector.

The x-ray source was produced by focusing the 60 fs Ti:Sapphire facility laser, centered at 805 nm, onto a 100 um thick titanium or copper foil. The laser energy was varied between 0.1 and 5 J which produced an x-ray source dominated by either the titanium K_α x rays, 4.5 keV, or the copper K_α x rays, 8.05 keV, as determined from the spectra obtained with a single hit x-ray CCD camera. The spectrum from a 92 mJ shot on a titanium target is shown in Figure 5. For testing with a visible/ultraviolet pump source

at 403 nm, a crystal was used to frequency double the Ti:Sapphire laser which then illuminated the CdSe semiconductor.

A composite of raw data from one of the Ti K_α x-ray pump series is shown in Figure 6. Figure 6a shows the measured signal with the probe beam incident on the CdSe with no Ti K_α pump x rays present and the zero order and negative orders blocked on the Fourier plane filter. This signal represents the probe light which is scattered by the surfaces and internal structure of the CdSe semiconductor. Figure 6b represents the apodized zero order signal with the probe beam incident on the CdSe with no Ti K_α pump x rays and only the negative orders blocked on the Fourier plane filter. Figure 6c shows the diffracted signal with the probe beam incident on the CdSe at the same time as the 4.5 keV x-ray pump source and the zero order and negative orders blocked on the Fourier plane filter. The images are analyzed by subtracting the normalized scattered signal, Fig. 6a, from both the probe image, Fig. 6b, and from the diffracted signal, Fig. 6c. The difference between the diffracted signal and the scattered signal with no pump, Fig. 6c minus Fig. 6a, is then divided by the difference between the spatial profile of the zero order probe beam and the scattered signal with no pump beam, Fig. 6b minus Fig. 6a. The square root of this ratio, shown in Fig. 7, is then proportional to the transient phase produced in the CdSe and hence the spatial profile of the x-ray flux.

The spatial profile of the x-ray flux in figure 7 can then be analyzed to determine the modulation transfer function, MTF, of the framing camera as configured in this experiment. This was accomplished in two ways. In the first method, a series of bar patterns were implemented in the x-ray grating/mask with the pitch of the bar patterns decreasing by a factor of two between each set of bars. By taking lineouts of the bar

patterns the MTF can be determined as a function of cycles/mm. In this case the percent MTF at 2 cycles/mm was defined as one and the results of this analysis are shown in Fig. 8 as discreet circles. For the second method, the edge at the upper left corner of the letter N in the grating/mask shown in Fig. 4 was used to determine the MTF. The MTF is equal to the absolute value of the Fourier transform of the derivative of the edge spread function. The edge spread function in this case was a horizontal lineout across the left edge of the N which was averaged in the vertical direction. The MTF calculated from the edge spread function is denoted by the dashed black line in Fig. 8. The MTF and hence the spatial resolution in this case is limited by the diameter of the circle in the Fourier plane. By either removing the Fourier filter or by decreasing the pitch of the x-ray grating and correspondingly increasing the diameter of the circle by the same amount in the Fourier plane the spatial resolution would be increased. For instance changing the pitch of the grating from its current 50 lp/mm to 250 lp/mm and increasing the diameter of the circles in the Fourier plane by the same factor of five would increase the spatial resolution to ~ 5 um.

For each shot the diagnostic measured two frames displaced in time by 5 ps. A time sequence composed from two shots, two frames on each shot, is shown in Figure 9. These images have been normalized by the zero order undiffracted beam. This sequence begins with the probe beam incident on the CdSe semiconductor before the x rays from the laser-produced plasma are incident on the front side of the semiconductor and ends with the probe beam incident after x rays have impinged upon the CdSe semiconductor. A camera was also employed to measure the Fourier plane images. This camera was used to assess the ratio between the scattered light in the zero and first order beams to

determine the level of the transient phase grating driven in the semiconductor. Previous experiments in conjunction with simulations determined that the energy in the first order, E_1, of a uniform grating, made with the same lithography mask as the current grating/mask, relative to the energy in the zero order, E_0, was equal to $E_1/E_0 = 0.067(\phi)^2$, where ϕ is the phase amplitude of the grating in radians.[16] From the ratio of the energy scattered in the zero and first orders in the Fourier camera, it was determined that the transient grating in Fig. 9a had a phase amplitude of 0.01 radians, Fig. 9b had a phase amplitude of 0.03 radians, Fig. 9c had a phase amplitude of 0.54 radians and Fig. 9d had a phase amplitude of 0.47 radians. From this time series it is evident that the rise time of the modulation in the probe beam is less than the 1.7 ps inter-frame time between Fig. 9b and Fig. 9c.

The multiframe capability of a CdSe semiconductor was also tested in the visible/UV region by frequency doubling the 805 nm Ti:Sapphire laser. In this case an aluminum grating deposited on a quartz substrate was used to modulate the incident flux on the semiconductor. This grating did not contain resolution test patterns but rather only the central NIF logo which was common to the x-ray grating. A time sequence of diffracted images from this exposure is shown in Fig. 10. Each image is delayed relative to the image above by 1.67 ps such that Fig. 10a represents the first shot with a delay of τ and Fig. 10b represents the second shot with the probe delayed τ+1.67 ps relative to Fig. 10a, etc.. The vertical dashed line separates the two frames on a given shot. The image to the left of the dashed line has its probe delayed by 5 ps relative to the image on the right. Again a camera located in the Fourier plane was used to determine the phase amplitude of the transient grating as a function of delay between the probe and the pump source.

Figure 11 then shows the time-dependent phase amplitude of the transient grating. The line is a fit to the experimental points and has the form

$$\text{Phase} = 0.0615 * \exp(-(\tau - 1.9)/60.1)/(1 + \exp(-(\tau - 1.9)/1.)), \quad (1$$

where τ is the time in ps. This shows that the decay of the transient phase has an exponential form with a decay time of ~60 ps. The fit, Eq. 1, to the experimental points has a rise from 20% to 80% of 2.6 ps.

In summary, a solid state framing camera has been developed and tested in the visible and hard x-ray regime. The camera currently records two frames with a temporal separation between the two frames of 5 ps, which could easily be varied. We employed polarization techniques for this design to realize the two frames for the framing camera, however, it would be straightforward to use alternative techniques to enable many more temporal frames. For this experiment a CdSe semiconductor driven by a pump, x-ray or visible, was used to spatially and temporally modulate the probe beam. This particular semiconductor enables continuous operation of the framing camera from the visible/near infrared to the hard x-ray regime, 10's of keV. The use of a narrower bandgap semiconductor would enable the extension of this technique well into the long-wavelength infrared spectrum, down to 12 um using $Hg_{0.8}Cd_{0.2}Te$ for instance. This diagnostic measured transient phase amplitudes, driven by the x-ray flux, ranging between 0.01 radians to 0.54 radians, the upper limit of which was limited by the available x-ray flux from the source. Improvements in sensitivity can be realized by probing the semiconductor much closer to the bandgap, choosing a semiconductor such as GaAs which has significantly less internal scattering and which is easier to polish to achieve a higher surface quality(less scattering), decreasing the pitch of the modulating

grating(also leads to improved spatial resolution) to move the diffracted signal to a region of lower scatter and employing an interferometric detection scheme.

This work was performed under the auspices of the U.S. Department of Energy by Lawrence Livermore National Laboratory under Contract DE-AC52-07NA27344. The authors would like to acknowledge the JLF staff for their support of these experiments and in particular J. Bonlie, C. Filip, C. Cadwalader, R. Costa, G. Freeze and S. Maricle. We also wish to acknowledge G. Loomis, P. Thelin and J. Dela Fuente for optical coating, polishing and manufacturing support.

REFERENCES

[1] Henry N. Chapman, Anton Barty, Michael J. Bogan, Sebastien Boutet, Matthias Frank, Stefan Hau-Riege, Stefano Marchesini, Bruce W. Woods, Sasa Bajt, W. Henry Benner, Richard A. London, Elke Plonjes, Marion Kuhlmann, Rolf Treusch, Stefan Dusterer, Thomas Tschentscher, Jochen R. Schneider, Eberfard Spiller, Thomas Moller, Christoph Bostedt, Matthias Hoener, David A. Shapiro, Keith O. Hodgson, David Van Der Spoel, Florian Burmeister, Mangus Bergh, Carl Caleman, Gosta Huldt, M. Marvin Seibert, Filipe R. N. C. Maia, Richard W. Lee, Abraham Szoke, Nicusor Timneanu and Janos Hajdu, "Femtosecond diffractive imaging with a soft-X-ray free-electron laser," Nature Physics **2** (2006)

[2] Anton Barty, Sebastien Boutet, Michael J. Bogan, Stefan Hau-Riege, Stefano Marchesini, Klaus Sokolowski-Tinten, Nikola Stojanovic, Ra'anan Tobey, Henri Ehrke, Andrea Cavalleri, Stefan Dusterer, Matthias Frank, Sasa Bajt, Bruce W. Woods, M. Marvin Seibert, Janos Hajdu, Rolf Treusch and Henry N. Chapman, "Ultrafast single-shot diffraction imaging of nanoscale dynamics," Nature Photonics **2**, 415 (2008)

[3] C. M. Gunther, B. Pfau, R. Mitzner, B. Siemer, S. Roling, H. Zacharias, O. Kutz, I. Rudolph, D. Schondelmaier, R. Treusch and S. Eisebitt, "Sequential femtosecond X-ray imaging," Nature Photonics **5**, 99 (2011).

[4] S. Roy, D. Parks, K. A. Seu, R. Su, J. J. Turner, W. Chao, E. H. Anderson, S. Cabrini and S. D. Kevan, "Lensless X-ray imaging in reflection geometry," Nature Photonics **5**, 243 (2011)

[5] Henry N. Chapman and Keith A. Nugent, "Coherent lensless X-ray imaging," Nature Photonics **4**, 833 (2010).

[6] Fienup, J. R., "Reconstruction of an object from modulus of its Fourier transform," *Opt. Lett.* **3**, 27–29 (1978)

[7] Gerchberg, R. W. and Saxton, W. O., "Practical algorithm for determination of phase from image and diffraction plane pictures," *Optik* **35**, 237–246 (1972).

[8] C. Stoeckl, J. A. Delettrez, R. Epstein, G. Fiksel, D. Guy, M. Hohenberger, R. K. Jungquist, C. Mileham, P. M. Nilson, T. C. Sangster, M. J. Shoup III, and W. Theobald, "Soft x-ray backlighting of direct-drive implosions using a spherical crystal imager on OMEGA," Rev. Sci. Instrum. **83**, 10E501 (2012).

[9] O. L. Landen, D. R. Farley, S. G. Glendinning, L. M. Logory, P. M. Bell, J. A. Koch, F. D. Lee, D. K. Bradley, D. H. Kalantar, C. A. Back, and R. E. Turner, "X-ray backlighting for the National Ignition Facility," Rev. Sci. Instrum. **72**, 627 (2001).

[10] D. K. Bradley, P. M. Bell, O. L. Landen, J. D. Kilkenny, and J. Oertel, "Development and characterization of a pair of 30–40 ps xray framing cameras," Rev. Sci. Instrum. **66**, 716 (1995).

[11] Bourgade, J. L., Marmoret, R., Darbon, S., Rosch, R., Troussel, P., Villette, B., Glebov, V., Shmayda, W. T., Gomme, J. C., Tonqueze, Y. L., Aubard, F., Baggio, J., Bazzoli, S., Bonneau, F., Boutin, J. Y., Caillaud, T., Chollet, C., Combis, P., Disdier, L., Gazave, J., Girard, S., Gontier, D., Jaanimagi, P., Jacquet, H. P., Jadaud, J. P., Landoas, O., Legendre, J., Leray, J. L., Maroni, R., Meyerhofer, D. D., Miquel, J. L., Marshall, F. J., Masclet-Gobin, I., Pien, G., Raimbourg, J., Reverdin, C., Richard, A., Cervens, D. R. d., Sangster, C. T., J. P. Seaux3, G. S., Stoeckl, C., Thfoin, I., Videau, L. and Zuber, C.,

"Diagnostics hardening for harsh environment in Laser Mégajoule," Rev. Sci. Instrum. **79** , 10F301 (2008).

[12] Z. G. Yu, Srini Krishnamurthy and Shekhar Guha, "Photoexcited-carrier-induced refractive index change in small bandgap semiconductors," J. Opt. Soc. Am. B **23**, 2356 (2006).

[13] Robert J. Vanderbei, David N. Spergel and N. Jeremy Kasdin, "Circularly Symmetric Apodization via Star-Shaped Masks," ApJ **599**, 686 (2003).

[14] E. Hugot, M. Ferrari, K. ElHadi, A. Costille K. Dohlen, P. Rabou, P. Puget, and J. L. Beuzit, "Active optics methods for exoplanet direct imaging," A&A **538**, A139 (2012).

[15] Christopher J. Walsh, Achim J. Leistner, and Bozenko F. Oreb, " Power spectral density analysis of optical substrates for gravitational-wave interferometry," Appl. Opt., **38**, 4790 (1990).

[16] K. L. Baker, R. E. Stewart, P. T. Steele, S. P. Vernon, and W. W. Hsing, "Ultrafast semiconductor x-ray detector," Appl. Phys. Lett. **101**, 031107 (2012).

FIGURE CAPTIONS

Figure 1 Single leaf of the discreet Blackman apodizer implemented for the x-ray framing camera.

Figure 2 Wave optics simulations of the Fourier plane in the case where the x-ray flux produced a transient grating in the CdSe with an amplitude of 0.00628 radians. Figure 2a represents the Fourier plane for a probe beam with an unapodized hard circular aperture. In this case the diffracted signal from the transient grating is not apparent above the diffraction pattern of the probe beam. Figure 3a represents the Fourier plane for a probe beam with a continuous Blackman apodized probe beam. In this case the diffracted signal from the transient grating is readily apparent above the diffraction pattern of the Blackman apodized probe beam.

Figure 3 Experimental geometry used to measure the two-dimensional x-ray flux produced by the laser-plasma source at two separate times. Labels in the figure are: mirror(M), lens (L), beam splitter(BS), charge coupled device(CCD), beam displacer(BD), Fresnel biprism(FB), nonpolarizing beamsplitter(NPBS) and half waveplate ($\lambda/2$).

Figure 4 X-Ray Grating/Mask used for two-dimensional imaging diagnostics. The gray regions indicate where ~10 um of gold blocked the x-rays and the open areas allowed the x-rays to impinge upon the semiconductor.

Figure 5 Histogram of the x-ray spectrum driven when the laser interacts with the titanium target. This spectrum was taken with a laser energy of 92 mJ.

Figure 6 Composite raw data images. Figure 6a shows the measured signal with the probe beam incident on the CdSe with no x-ray pump signal and the zero order and negative orders blocked on the Fourier plane filter. This signals represents the light which is scattered by the surfaces and internal structure of the CdSe semiconductor. Figure 6b represents the apodized zero order signal with the probe beam incident on the CdSe with no x-ray pump signal and only the negative orders blocked on the Fourier plane filter. Figure 6c shows the diffracted signal with the probe beam incident on the CdSe at the same time as the x-ray pump signal and the zero order and negative orders blocked on the Fourier plane filter.

Figure 7 Processed x-ray framing camera signal with 5 ps inter-frame time between the upper and lower frames. This image was taken with Ti k_{α} x rays backlighting a resolution pattern/grating.

Figure 8 Modulation transfer function produced from the bar patterns in the x-ray grating/mask.

Figure 9 Sequence of two-dimensional images obtained from x-ray pumped, 4.5 keV, CdSe.

Figure 10 Sequence of two-dimensional diffracted images obtained from optically pumped, 403 nm(3.1 eV), CdSe. Each image is delayed relative to the image above by 1.67 ps such that Fig. 10a represents the first shot with a delay of τ and Fig. 10b represents the second shot with the probe delayed τ+1.67 ps relative to Fig. 10a, etc.. The vertical dashed line separates the two frames on a given shot. The image to the left of the dashed line has its probe delayed by 5 ps relative to the image on the right.

Figure 11 Temporal decay of the transient phase grating excited in CdSe via optical pumping at 403 nm(3.1 eV). Each point represents a separate shot with the delay in the probe beam adjusted between each shot.

FIGURES

KL Baker

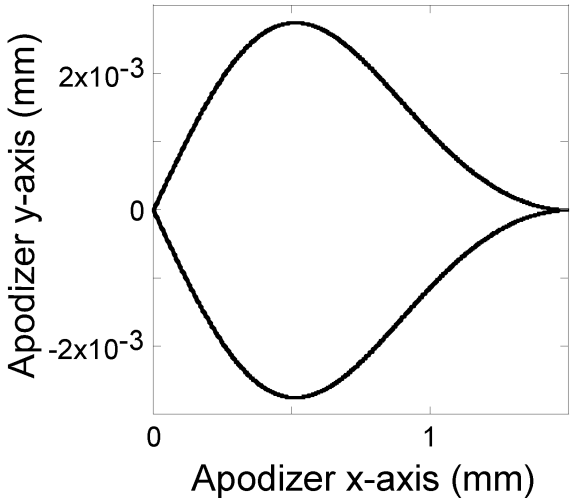

Figure 1

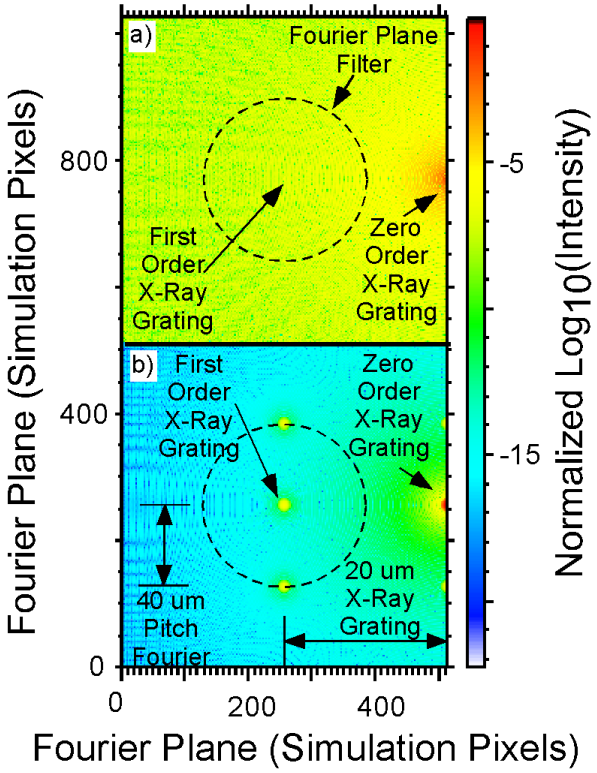
a)
Fourier Plane
Filter
First
Order
X-Ray
Grating
Zero
Order
X-Ray
Grating
b)
First
Order
X-Ray
Grating
Zero
Order
X-Ray
Grating
40 um
Pitch
Fourier
20 um
X-Ray
Grating
800
400
0
0
200
400
Fourier Plane (Simulation Pixels)
Fourier Plane (Simulation Pixels)
-5
-15
Normalized Log10(Intensity)

Figure 2

KL Baker

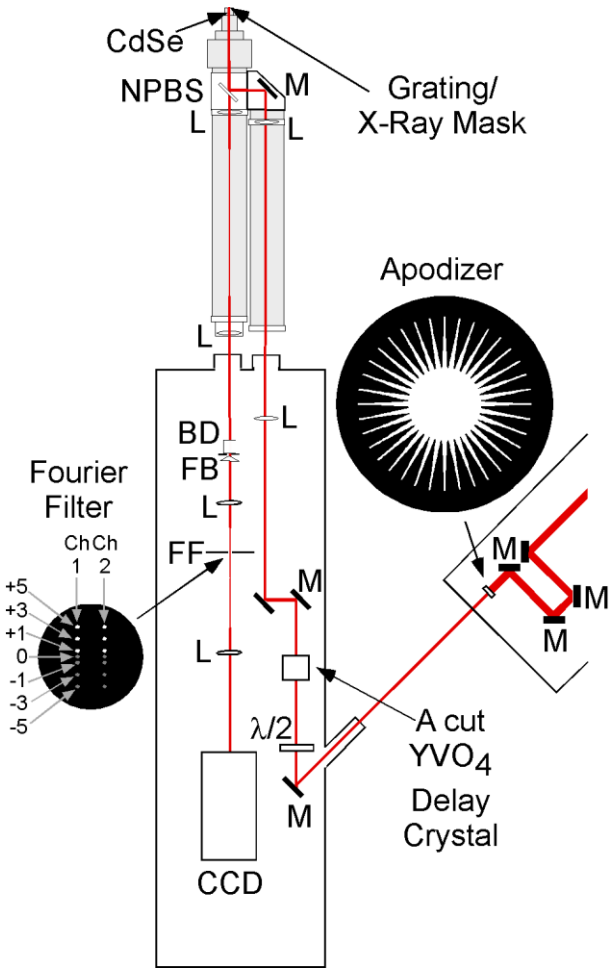

Figure 3

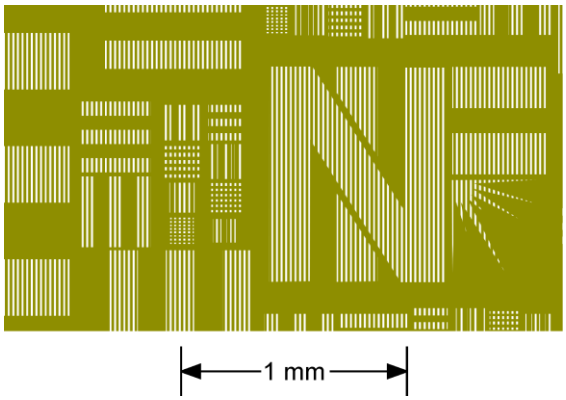

Figure 4

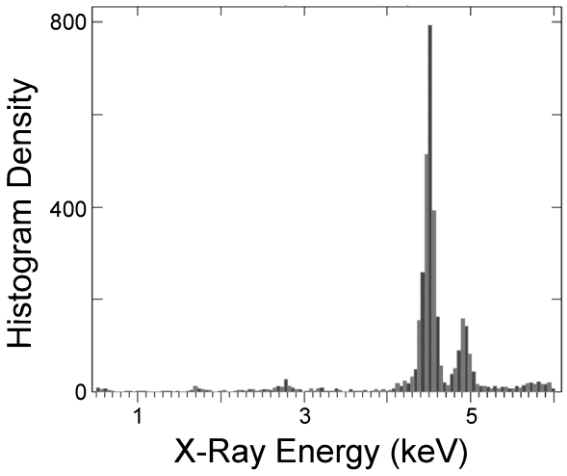

Figure 5

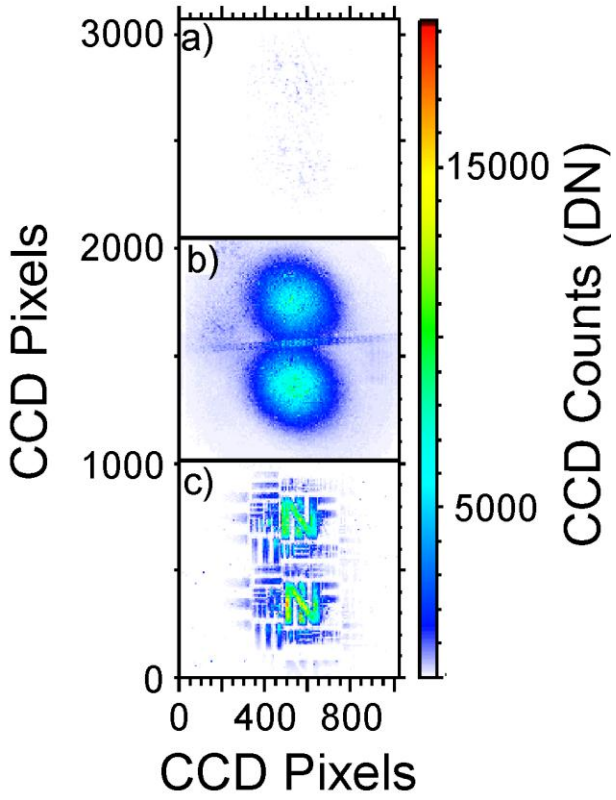
3000
2000
1000
0
a)
b)
c)
0
400
800
CCD Pixels
CCD Pixels
15000
5000
CCD Counts (DN)

Figure 6

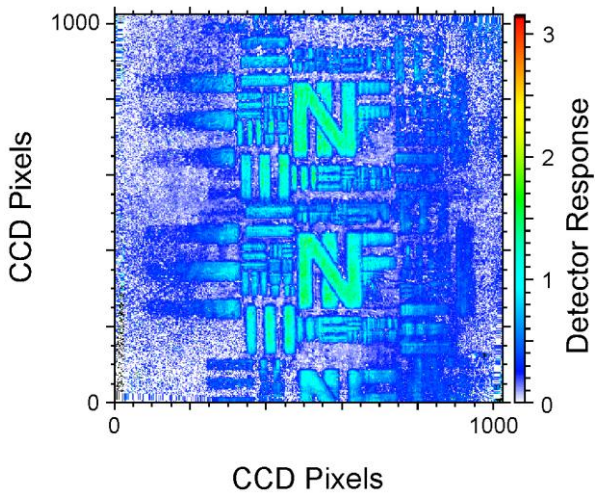

Figure 7

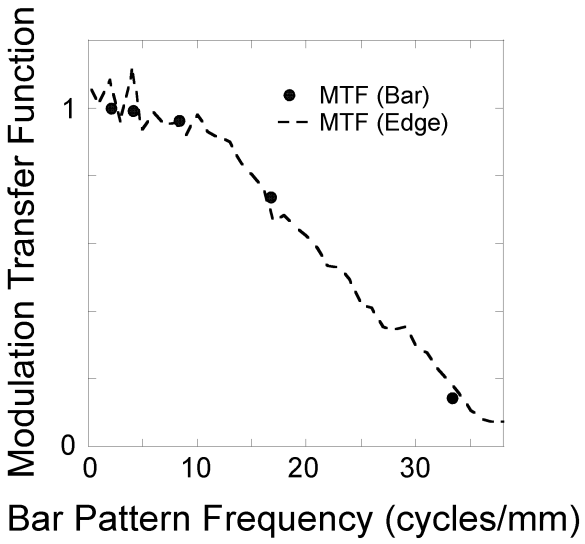
Modulation Transfer Function
1
0
0
10
20
30
MTF (Bar)
MTF (Edge)
Bar Pattern Frequency (cycles/mm)

Figure 8

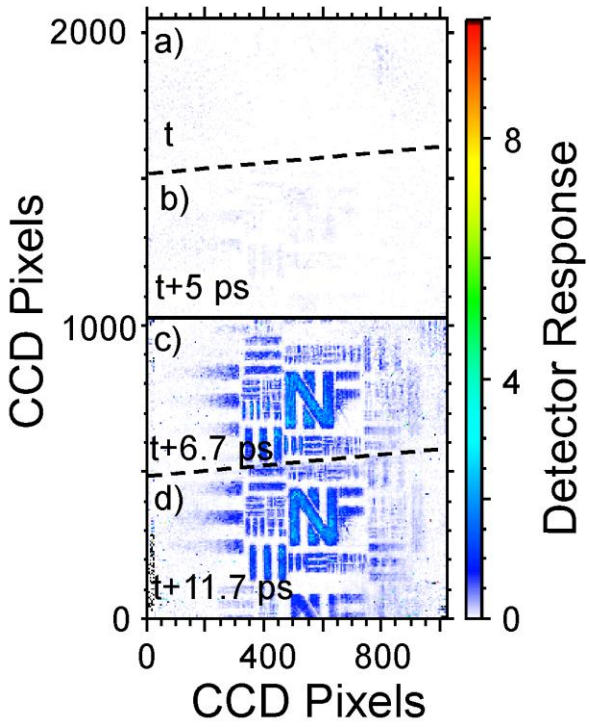
2000
1000
0
a)
t
b)
t+5 ps
c)
t+6.7 ps
d)
t+11.7 ps
0
400
800
CCD Pixels
CCD Pixels
8
4
0
Detector Response

Figure 9

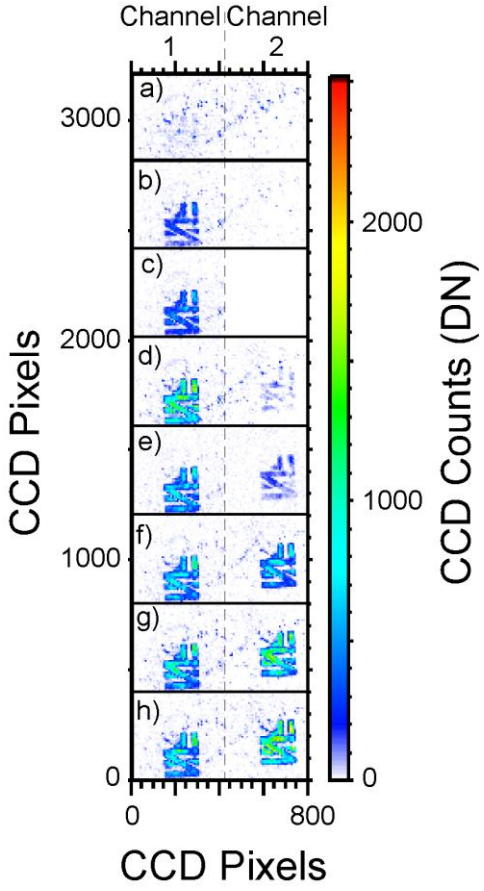
Channel 1
Channel 2
a)
b)
c)
d)
e)
f)
g)
h)
3000
2000
1000
0
0
800
CCD Pixels
CCD Pixels
2000
1000
0
CCD Counts (DN)

Figure 10

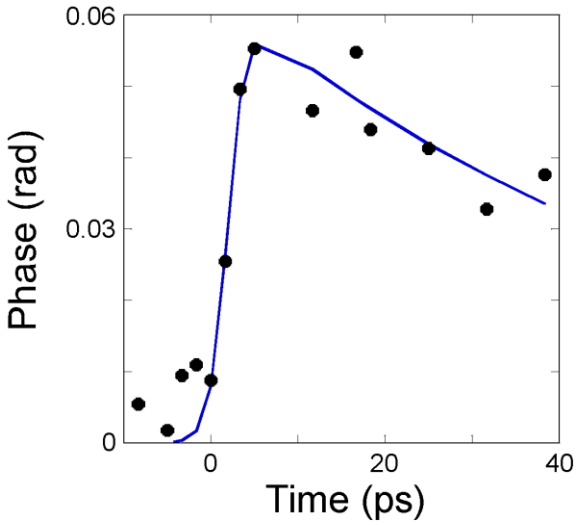

Figure 11